

MODELING AND VALIDATION OF FORCED CONVECTION SUBCOOLED BOILING

D. R. Shaver and M. Z. Podowski

Center for Multiphase Research

Rensselaer Polytechnic Institute, Troy, NY, USA

shaved2@rpi.edu, podowm@rpi.edu

ABSTRACT

To support the development of next-generation nuclear power reactors, new mechanistic based computational models of reactor thermal-hydraulics need to be formulated, tested, and implemented. A new subcooled boiling model has been developed with the objective of reducing dependence on empirical correlations. The model is able to accurately account for vapor generation on a heated wall as well as for condensation-induced heat and mass transfer from vapor to subcooled liquid. This model represents a substantial improvement over previous models and is part of an ongoing effort [1]. The new model has been extensively validated against experiments covering a wide range of fluids, geometries, and flow conditions.

The accuracy of subcooled boiling models is dependent on a consistent formulation of diabatic multiphase flow. A complete formulation for a dispersed field model is presented, along with a consistent set of interfacial heat, mass, and momentum transfer models. The drag and virtual mass forces have been formulated using well-accepted expressions. Novel formulations of the turbulent dispersion force and a relationship for a near-wall-varying lift coefficient are presented.

The complete subcooled boiling model has been implemented in the state-of-the-art computational multiphase fluid dynamics solver, NPHASE-CMFD. The experiments used in model validation cover flows of water, heavy water, and refrigerant. The geometrical configurations of heated channels include circular pipes, annuli, and rectangular conduits [2, 3, 4, 5]. The experimental conditions used in the present study correspond to a wide range of flow rates, pressures and heating rates. The same model has been applied consistently to all experiments of reference. That is, the model has not been calibrated to any specific experimental data set, and any adjustments in the modeling parameters between the simulations of different experiments have been made based on *a priori* analysis. This demonstrates the truly predictive nature of the presented model of subcooled boiling. Comparisons are shown between the predictions and experimental data for the axial and radial distributions of both vapor phase volume fraction and liquid subcooling. The observed agreement between the model and the experimental data is quite good for all simulated experiments.

KEYWORDS

Subcooled boiling, Thermal non-equilibrium, Computational multiphase fluid dynamics

1. INTRODUCTION

The modeling of subcooled boiling is a significant challenge. Predicting the transition from single phase flow to nucleate boiling involves several complex phenomena which must be modeled accurately. This presents an interesting problem in that many of the underlying physical phenomena are dependent on each other. This makes individual phenomena difficult to isolate, e.g. the vapor generation rate from the

condensation rate. It is important to accurately predict these phenomena independently as small changes in one or the other can have significant impacts on the overall characteristics of a two-phase flow.

The objective of this work is to present the results of model development and testing in the simulation of subcooled boiling flows. The proposed model of subcooled boiling is built upon the framework established by the Kurul-Porodowski model [6] and accounts for the vapor generation due to boiling, condensation of bubbles attached to the wall, and interfacial energy, mass, and momentum transfer between liquid and vapor phases at non-equilibrium conditions. The initial scope of the subcooled boiling model is to be able to predict flows of interest in commercial PWRs.

The Kurul-Podowski model has been well-accepted and has been adapted for use in several commercial CFD codes, but it relies heavily on empirical correlations. This dependence has been observed by several other authors who note the applicability of the model is limited by the range of the constituent correlations [7, 8, 9]. In particular, the model relies on empirical expressions for bubble diameter, nucleation site density, and ebullition frequency. All three of these parameters play particularly important roles in determining the boiling heat flux and an accurate prediction of them is paramount to the performance of the model. The primary objective of this work is to present a model with reduced dependence on and sensitivity to empirical correlations.

1.1. Experimental Data

In order to validate the subcooled boiling model, a wide range of experimental data has been selected. For subcooled boiling flows of interest in commercial PWRs, typically the volume fraction of the vapor phase remains small (<0.3) and the flow behaves predominantly as a bubbly flow. Additionally, due to the high pressure, the bubbles themselves remain small (<1 mm) and spherical. Four experiments have been chosen, covering different fluids, geometries, and flow conditions, but remaining within the above given criteria. These are the experiments of Bartolomei and Chanturiya [2], Rouhani [3], St. Pierre [4], and one of the DEBORA [5] experiments. Descriptions and details of the subcooled boiling experiments are detailed in Table I and Table II.

The experiments of Bartolomei, Rouhani, and St. Pierre all provide axial profiles of the average vapor volume fraction which is used as one criterion for evaluating the subcooled boiling model. The

Table I. Description of the subcooled boiling experiments

Experiment	Fluid	Geometry	Dimensions (mm)	Heated Length (m)
Bartolomei	water	Circular	15.4 diameter	2
Rouhani	heavy water	Annulus	12 ID, 25 OD	3
St. Pierre	water	rectangular	44.5x11.1	1.53
DEBORA	R12	Circular	19.2 diameter	3.5

Table II. Conditions for the subcooled boiling experiments

Experiment	G (kg/m ² -s)	q'' (kW/m ²)	ΔT_{in} (K)	P (MPa)
Bartolomei	900	570	-60	4.5
Rouhani	1450	130*	-41	3
St. Pierre	640	144	-5.2	2.8
DEBORA	1986	73.89	-18	2.6

*The heat flux is applied to the inner wall of the annulus

experiments of St. Pierre and DEBORA provide transverse profiles of vapor volume fraction. This was essential to determine the accuracy of the interfacial force models, particularly since these are developing flow conditions.

The vapor volume fraction was measured using gamma-densitometry for the experiments of Bartolomei, Rouhani, and St. Pierre. All three utilized a wide-beam to measure the cross-sectional average volume fraction. However, for the experiment of St. Pierre, a narrow beam was also used to find a local, width-average of vapor volume fraction at various points across the channel thickness. The width average measurements were then integrated to compare to the cross-sectional average measurements. Both sets of data points are used for comparison. For the DEBORA experiment, an optical probe technique was used.

Measurements of the liquid subcooling are provided by Bartolomei, Rouhani, and the DEBORA experiment. For Bartolomei's and Rouhani's experiments, axial profiles of the centerline temperature and bulk temperature are presented. For the DEBORA experiment, radial measurements of the liquid subcooling are available. The radial profiles of liquid subcooling are necessary to evaluate the accuracy of the interfacial heat and mass transfer model.

2. TWO PHASE FLOW MODELING

The subcooled boiling model has been implemented as part of a RANS-based, ensemble-averaged formulation of a two-fluid model (for details of the ensemble-averaged formulation see [10]). The state-of-the-art computational multiphase fluid dynamics (CMFD) code, NPHASE-CMFD [11], provides the framework for implementing the model. NPHASE-CMFD has been used due its proven capability in the simulation of a variety of multiphase flows [12, 13, 14] and due to the robustness of the numerical solver.

NPHASE-CMFD solves the conservation equations for mass, momentum, and the interfacial jump condition in either a coupled or segregated manner. It also solves the conservation of energy and turbulence quantity transport equations. It is notable that the coupled solver in NPHASE-CMFD couples together the mentioned equations for *all* simulated fields or fluid components and has the built-in capability of solving multiple (i.e. more than two) fields or fluid components. Since it was developed with the intention of simulating multiphase flows, NPHASE-CMFD includes enhanced numerical techniques allowing for highly stable implementations of interfacial interactions.

2.1. Governing Equations

NPHASE-CMFD provides the foundation for performing simulations of complex multi-phase flows. This includes the formulation of the governing conservation equations as well as the transport equations for turbulence quantities. The forms of the governing equations used in this work are presented below formulated for fluid-component 'j' which interacts with fluid component 'k'. The conservation equations for mass, momentum, and energy are

$$\frac{\partial}{\partial t} \alpha_j \rho_j + \nabla \cdot \alpha_j \rho_j \bar{u}_j = \Gamma_{k-j}''' - \Gamma_{j-k}''' \quad (1)$$

$$\frac{\partial}{\partial t} \alpha_j \rho_j \bar{u}_j + \nabla \cdot \alpha_j \rho_j \bar{u}_j \bar{u}_j = -\alpha_j \nabla P_j + \alpha_j \nabla \cdot \underline{\tau}_{lam,j} + \underline{\tau}_{turb,j} + \alpha_j \rho_j \bar{g} + \sum \bar{M}_{k-j}''' + \Gamma_{k-j}''' \bar{u}_k - \Gamma_{j-k}''' \bar{u}_j \quad (2)$$

$$\frac{\partial}{\partial t} \alpha_j \rho_j h_j + \nabla \cdot \alpha_j \rho_j \bar{u}_j h_j = \nabla \cdot \left[\alpha_j \bar{q}_{lam,j}'' + \bar{q}_{turb,j}'' \right] + q_{k-j}'' A_{kj}''' + \Gamma_{k-j}''' h_k - \Gamma_{j-k}''' h_j \quad (3)$$

Note that viscous dissipation as well as mechanical effects are neglected in the energy equation and a dispersed field model is used. The dispersed field model assumes the interfacial and dispersed field pressures and shears are equal to the continuous field pressure and shear. A more general formulation of the equations is available in the NPHAS-CMFD manual [11].

The conservation equations are combined with a K- ε turbulence model. The transport equations for the turbulent kinetic energy, K , and the turbulence dissipation rate, ε , are included in NPHASE-CMFD as

$$\frac{\partial}{\partial t} \alpha_c \rho_c K_c + \nabla \cdot \alpha_c \rho_c \vec{u}_c K_c = \nabla \cdot \left[\alpha_c \mu_c + \mu_{turb,c} \nabla K_c \right] + \alpha_c \Phi_c - \rho_c \varepsilon_c \quad (4)$$

$$\frac{\partial}{\partial t} \alpha_c \rho_c \varepsilon_c + \nabla \cdot \alpha_c \rho_c \vec{u}_c \varepsilon_c = \nabla \cdot \left[\alpha_c \mu_c + \mu_{turb,c} \nabla \varepsilon_c \right] + \alpha_c \frac{\varepsilon_c}{K_c} C_1 \Phi_c - C_2 \rho_c \varepsilon_c \quad (5)$$

Note that the subscript ‘ j ’ denoting a general fluid component has been replaced with ‘ c ’, denoting the continuous fluid component. While NPHASE-CMFD includes the capability of modeling turbulence in general for multiple fluid components, in this work turbulence is assumed to only be significant for the continuous fluid component. The shear production rate for the continuous fluid is given by

$$\Phi_c = \mu_c + \mu_{turb,c} \nabla \vec{u}_c \cdot \nabla \vec{u}_c + \nabla \vec{u}_c^T \quad (6)$$

In addition to the above conservation and transport equations, NPHASE-CMFD provides a built-in bubble induced turbulence model [15]

$$\mu_{turb,c} = \frac{\rho_c C_\mu K_c^2}{\varepsilon_c} + C_{BI} D_b \rho_c \alpha_d \left| \vec{u}_d - \vec{u}_c \right| \quad (7)$$

where the coefficient for the bubble induced turbulence is constant at 0.6 and the subscript ‘ k ’ has been replaced with ‘ d ’, denoting the dispersed fluid component. This model accounts for induced turbulence as an increased shear-stress in the continuous phase caused by the displacement of the continuous fluid due to a passing bubble.

2.2. Interfacial Force Models

The hydrodynamic behavior of the vapor phase is described using interfacial force models for bubbly flow. Models for drag and virtual mass forces are implemented as commonly used formulations since these forces are well characterized and documented. The lift and turbulence dispersion forces have been modified specifically for simulation of non-fully developed multiphase flows typical of subcooled boiling. An explicit wall-lubrication force is not included, as the original formulation by Antal [16] describes its region of action as a very thin liquid layer near the wall which is not well resolved in the high Reynolds number RANS formulation.

The drag and virtual mass forces have been formulated using typical relations for small, spherical bubbles

$$\vec{M}_{D,c-d}''' = -\frac{3}{4} C_D \frac{\alpha_d}{D_b} \rho_c \vec{u}_d - \vec{u}_c \left| \vec{u}_d - \vec{u}_c \right| \quad (8)$$

$$\vec{M}_{VM,c-d}''' = -C_{VM} \alpha_d \rho_c \left[\vec{u}_d \cdot \nabla \vec{u}_d - \vec{u}_c \cdot \nabla \vec{u}_c \right] \quad (9)$$

where the virtual mass coefficient is constant at 0.5 and the drag coefficient varies according to the bubble Reynolds number, $Re_b = |\vec{u}_d - \vec{u}_c| \rho_c D_b / \mu_c$, as

$$C_D = \frac{24}{Re_b} \left(1 + 0.092 Re_b^{0.78} \right) \quad (10)$$

This represents a slight modification to more commonly used expressions [17]. This was done to better match experimental measurements of drag coefficient in the expected range of bubble Reynolds numbers.

The formulation of the lift force matches the original model proposed by Zun [18]

$$\vec{M}_{L,c-d}''' = -C_L \alpha_d \rho_c \left(\vec{u}_d - \vec{u}_c \right) \times \nabla \times \vec{u}_c \quad (11)$$

However, the lift coefficient has been modified within a single bubble diameter of the wall. Closer than one bubble radius, the lift coefficient is zero and farther away than one bubble diameter it takes its nominal value, $C_{L,0}$, which has been chosen as constant at 0.03 based on extensive parametric studies and comparison to experimental data [19] and is consistent with the work of Jiao and Podowski [20]. Between one bubble radius and one diameter, it is adjusted using the following cubic expression

$$\frac{C_L}{C_{L,0}} = \left[3 \left(\frac{2y}{D_b} - 1 \right)^2 - 2 \left(\frac{2y}{D_b} - 1 \right)^3 \right] \quad (12)$$

The presence of the wall itself disrupts the standard force-balance approach to momentum conservation. Small bubbles tend to remain practically rigid in shape due to surface tension effects and cannot overlap with the wall. The modification to the lift coefficient effectively suspends the radial force balance in the near-wall region as the lift force is the only force expected to push bubbles towards the wall in this region.

The turbulent dispersion force has been formulated in a manner consistent with recent work by Jiao and Podowski [20]

$$\vec{M}_{TD,c-d}''' = -C_{TD} \alpha_d \rho_c K_{max} \nabla \alpha_d \quad (13)$$

where K_{max} refers to the value of turbulent kinetic energy near the wall. Typical formulations of the turbulent dispersion force assume turbulence behaves isotropically and use the local value of turbulent kinetic energy. Near the wall, however, turbulence has been observed to be highly anisotropic with the stream-wise fluctuation rising sharply and the radial component remaining practically constant [21]. Formulating the turbulent dispersion force using K_{max} more closely reflects the relationship between the radial turbulent fluctuation and the radial force component. It is expected that the turbulent dispersion coefficient take a value between 0.4 and 0.6. In this work, a constant value of 0.5 has been used.

The complete set of interfacial force models, including drag, virtual mass, lift, and turbulent dispersion has been implemented in NPHASE-CMFD and validated against experimental data for adiabatic two-phase flows [5, 21].

2.3. Models for Heat and Mass Transfer

The original Kurul-Podowski model makes use of the heat flux partitioning concept to predict the single phase, boiling, and quenching, heat fluxes as well as the wall temperature [6]. A similar approach has been taken here based on a previously proposed concept [1]. In this approach, the heat flux is partitioned into only two components, the boiling and single phase heat fluxes

$$q_w'' = q_b'' + q_{1\phi}'' \quad (14)$$

where the boiling heat flux is determined by the local liquid subcooling and the fraction of the wall area available for boiling

$$q_b'' = A_b'' \frac{h_{fg}}{h_{fg}} q_w'' \quad (15)$$

The wall area fraction is determined from

$$A_b'' = \left(\frac{\Delta T_w - \Delta T_{nucl}}{\Delta T_{nb} - \Delta T_{nucl}} \right)^2 \quad (16)$$

where ΔT_w is the local wall superheat, ΔT_{nucl} is the minimum wall heat required for nucleation, and ΔT_{nb} is the wall superheat in well-established boiling. In this work, the Jens-Lottes correlation has been used for ΔT_{nb} . This relationship assumes the boiling area is proportional to the wall superheat and is similar in concept to relating the nucleation site density to the wall superheat. This approach eliminates a direct dependency on the local bubble size present in the Kurul-Podowski model.

The relationship for the single phase heat flux is retained unaltered from the Kurul-Podowski model

$$q_{1\phi}'' = H_{1\phi} \left[1 - A_b'' \frac{\Delta T_w - \Delta T_{l,p}}{\Delta T_w - \Delta T_{l,p}} \right] \quad (17)$$

where $\Delta T_{l,p}$ refers to the liquid superheat (negative) in the next-to-wall node. However, the local single phase heat transfer coefficient is determined using a modification to the temperature-law-of-the-wall [22] which better accounts for fluids with non-unity molecular Prandtl numbers.

$$H_{1\phi} = u_\tau \rho_l c_{p,l} \left[y_{LSL}^+ Pr_l^{\frac{2}{3}} + \frac{Pr_{turb}}{\kappa} \ln \left(\frac{y_p^+ Pr_l^{\frac{1}{3}}}{y_{LSL}^+ Pr_l^{\frac{1}{3}}} \right) \right]^{-1} \quad (18)$$

Here, the subscript 'l' refers to the continuous liquid phase. Typically, these properties are evaluated at saturation. The boiling rate per unit wall area is then determined from the boiling heat flux

$$\Gamma_{w,evap}'' h_{fg} = q_b'' \quad (19)$$

The basis of the presented subcooled boiling model is accounting for condensation of bubbles still attached to the boiling wall. These so-called "standing bubbles" are not large enough to lift-off from the wall, but protrude deep enough into the subcooled liquid that the condensation off the bubble surface

away from the wall is significant. The model formulation is based on determining the condensation number, which is defined as the ratio of the condensation rate to the boiling rate. This must always be less than or equal to unity.

$$Co \equiv \frac{\Gamma''_{w,cond}}{\Gamma''_{w,evap}} \leq 1 \quad (20)$$

The condensation number can be determined by considering the rate of convective heat transfer from a single standing bubble compared to the energy available from boiling

$$Co = \frac{6 H_{cond} \Delta T_l^*}{D_{lo} \rho_v f h_{fg}} \quad (21)$$

where D_{lo} is the bubble lift-off diameter. Note that this does not have to be (and probably should not be) identical to the bubble diameter away from the wall (D_b). In the Kurul-Podowski model, the boiling heat flux is strongly dependent on the local bubble size. This formulation removes that dependence in favor of the bubble size at lift-off, which can be estimated more consistently.

The average heat transfer coefficient and liquid subcooling surrounding a standing bubble is then evaluated as

$$H_{cond} \Delta T_l^* = \frac{1}{D_{lo}} \int_0^{D_b} H_{cond} \Delta T_l dy \quad (22)$$

This assumes the bubbles remain small and spherical and that the liquid temperature is distributed axisymmetrically around any single bubble. Since no single bubble is resolved in the RANS framework, the axisymmetric assumption is reasonable. The convective heat transfer coefficient can be evaluated from an appropriate correlation. In this work, the correlation proposed by Chen and Mayinger [23] has been used

$$H_{cond} = \frac{k_l}{D_{lo}} \left(2 + 0.6 Re_{w,b}^{\frac{1}{2}} Pr_l^{\frac{1}{3}} \right) \quad (23)$$

Where the bubble Reynolds number on the wall is evaluated assuming the standing bubbles have zero-velocity, $Re_{w,b} = u_l \rho_l D_{lo} / \mu_l$.

The energy available from heating is based on an expression for conservation of energy for the vapor phase. This requires an estimate of the ebullition frequency and the relationship recommended by Ceumern-Lindenstjerna is used [24] based on its inclusion as part of the original Kurul-Podowski model.

$$f = \sqrt{\frac{4 g \rho_l - \rho_v}{3 D_{lo} \rho_l}} \quad (24)$$

Once the bubbles lift-off from the wall, they are exposed to subcooled liquid and begin to condense. The interfacial condensation rate is determined from the volumetric heat transfer rate between the bubbles and the surrounding liquid

$$\Gamma'''_{cond} h_{fg} = q_l''' \quad (25)$$

where the interfacial heat transfer rate is determined based on a convective relationship

$$q_l''' = -\frac{6\alpha_v}{D_b} H_l \Delta T_l \quad (26)$$

And the heat transfer coefficient is again evaluated using the correlation proposed by Chen and Mayinger [23] based on the bubble Reynolds number.

$$H_l = \frac{k_l}{D_b} \left(2 + 0.6 Re_b^{1/2} Pr_l^{1/3} \right) \quad (27)$$

2.4. Bubble lift-off diameter

The condensation model is strongly dependent on an *a priori* prediction of the bubble size. There are numerous correlations and models for determining this, but they all show poor experimental agreement with errors commonly above 100%. Two correlations [25, 26] and a physically based model [27] have been used to determine the bubble lift-off diameter for the four chosen subcooled boiling experiments. The force balance approach of Sugrue & Buongiorno was modified to predict the lift-off diameter, rather than the departure diameter. The results of calculations are summarized in Table III. Interestingly, the physically based model of Sugrue & Buongiorno consistently predicts bubble size an order of magnitude less than the purely empirical correlations. It should be noted that this model relies on a number of underlying empirical expressions which themselves may not be applicable to the chosen subcooled boiling experiments.

Table III. Bubble lift-off size predictions for the subcooled boiling experiments

Experiment	Jensen & Memmel	Unal	Sugrue & Buongiorno	Experimental
Bartolomei	0.51	0.1	0.034	–
Rouhani	0.58	0.22	0.023	–
St. Pierre	0.52	0.17	0.052	–
DEBORA	0.13	0.93	0.0047	0.24*

All values presented in mm

*Extrapolated from near-wall data

The presented correlations predict a wide range of values for the bubble lift-off diameter, as expected. While these correlations are able to reasonably predict the bubble size for the experiments they were originally developed from, any attempt to extend them beyond their narrow ranges produces large errors. This is a strong indication of the difficulty in predicting the bubble size. Due to the wide range predicted, these values should be treated with some skepticism.

3. COMPARISONS TO EXPERIMENTAL DATA

The selected experimental data encompasses a variety of fluids, geometries, and flow conditions. For the experiments using water and heavy water, the properties were assumed to remain constant and evaluated for saturation conditions at the indicated system pressure for both vapor and liquid. As stated by Chen et al. [9], variation in properties can be significant for heated flows of refrigerants, however. To more accurately capture the effect of thermal non-equilibrium between phases, a model for the specific heat as a function of liquid temperature has been implemented. All other fluid properties were assumed constant for the refrigerant.

The formulation of the model of subcooled boiling as presented above is consistent between all presented experiments. The bubble sizes, both at lift-off and away from the heated wall, vary between experiments according to values presented in Table IV. The values for the DEBORA experiment were determined based on the measurements of the original experiment. The values for the other experiments were determined based on a combination of physical reasoning as well as parametric testing, discussed in section 4.1.

Table IV. Summary of bubble sizes used in simulations

Experiment	D_{lo} (mm)	D_b (mm)
Bartolomei	0.5	0.75
Rouhani	0.6	0.75
St. Pierre	0.7	0.75
DEBORA	0.24*	0.5*

*Determined from experimental data

The results for the experiments of Bartolomei, Rouhani, and St. Pierre are presented with an uncertainty of +/- 0.025 for volume fraction and +/- 2 K for liquid subcooling. No quantification of uncertainty was available for these experiments and these values were chosen purely as a point of reference. The uncertainty values presented for the DEBORA experiment are consistent with an analysis performed by Yao and Morel [5].

The results for the Bartolomei's experiment are shown in Figure 1. The NPHASE-CMFD predicted average vapor volume fraction and centerline temperature are overlaid with the experimental data points. The agreement for the volume fraction can be seen to be quite good, as the simulation matches within +/- 0.025. Towards the end of the channel ($x/L > 0.85$) the predicted volume fraction continues increasing practically linearly, while the experimental volume fraction begins to taper off. This discrepancy is likely due to coalescence of bubbles in the flow away from the wall. The centerline temperature is slightly under-predicted by NPHASE-CMFD in this same region. This is the result of an insulating effect caused by diminished turbulence production. The effects on the overall simulation are minor, however.

The predicted volume fraction and liquid subcooling profiles for Rouhani's experiment are shown in Figure 2. The agreement for the volume fraction is very good prior to $x/L < 0.7$, after which the volume fraction is under-predicted. The liquid subcooling in this region is over-predicted, which is consistent with the under-prediction of volume fraction.

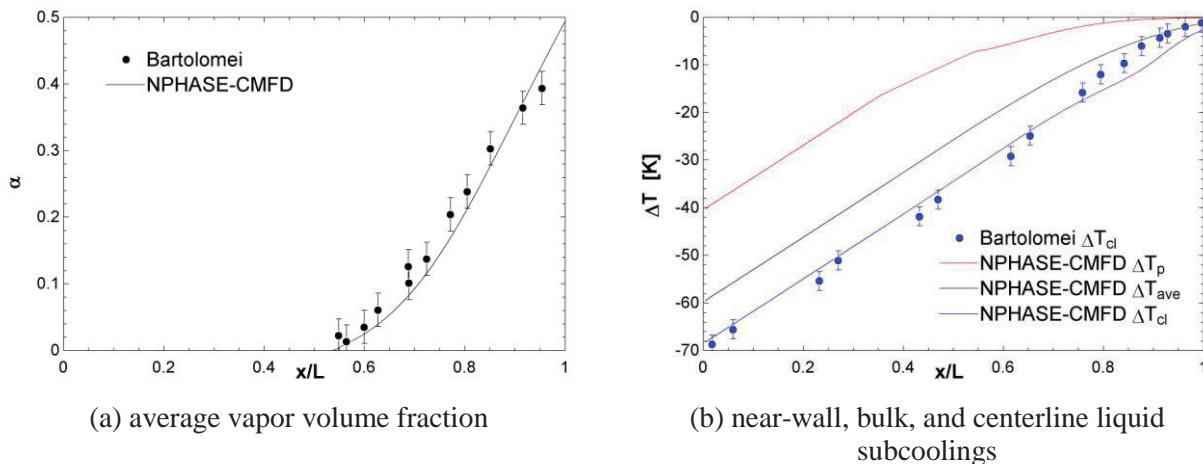
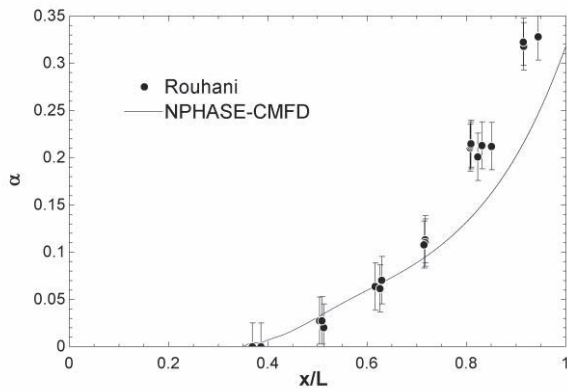
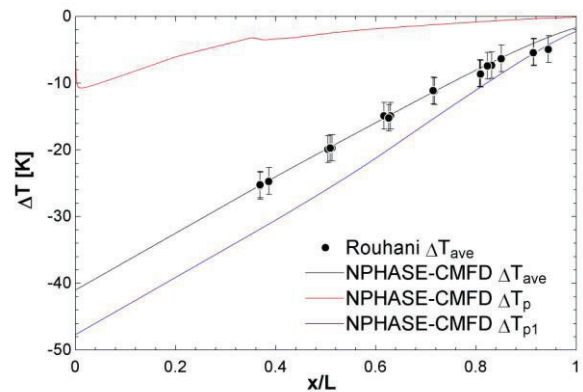


Figure 1. Results for the experiment of Bartolomei & Chanturiya



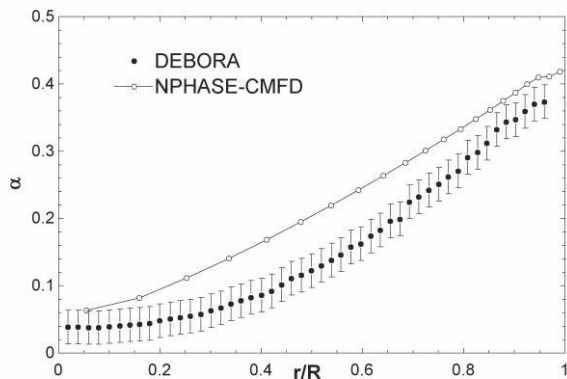
(a) average vapor volume fraction



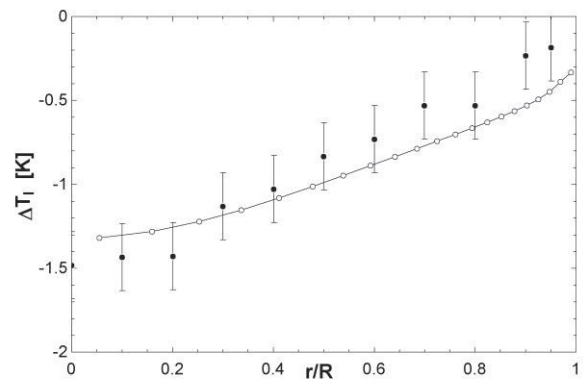
(b) near-wall and bulk liquid subcooling

Figure 2. Results for the experiment of Rouhani

Radial profiles of the predicted vapor volume fraction and liquid subcooling are presented in Figure 3 for the DEBORA experiment. The volume fraction profile agrees reasonably well with the experimental data, although it is consistently over-predicted by the model. Interestingly, the trend near the wall and value near the channel center are matched well. The gradient of volume fraction is larger for the experimental data in the range $0.7 > r/R > 0.9$. This could indicate a higher condensation rate than what is predicted by the model.



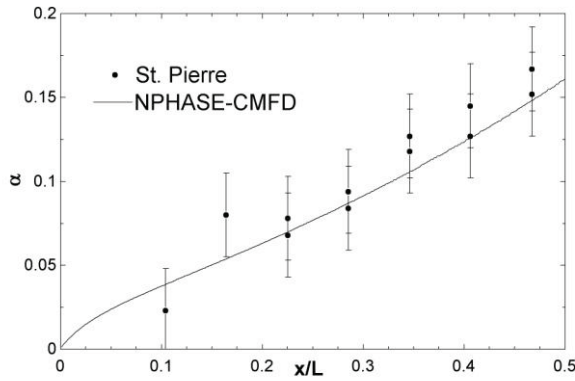
(a) radial profile of vapor volume fraction



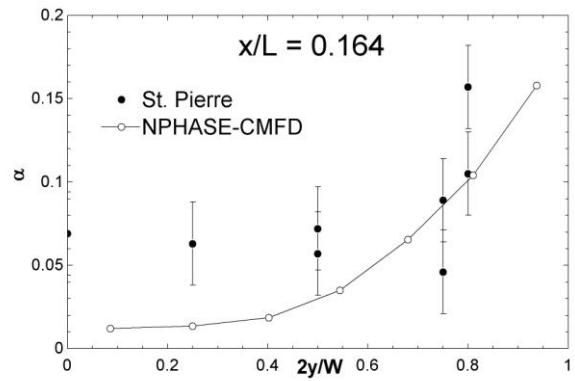
(b) radial profile of liquid subcooling

Figure 3. Results for the DEBORA experiment

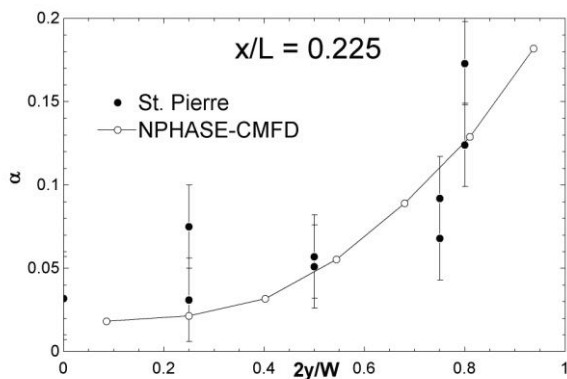
For the experiment of St. Pierre in a rectangular channel, a three-dimensional simulation was performed for one quarter of the geometry. The results for the average vapor volume fraction along the channel as well as transverse volume fraction profiles at different axial positions are shown in Figure 4 compared to experimental measurements. In the original experiment, St. Pierre measured the volume fraction along the entire width of the channel. Due to the inherent symmetry of a rectangular channel, the experimental data points have been reflected across the center plane of the domain. The transverse profiles are presented as line averages along the 44.5 mm channel thickness at different locations along the 11.1 mm channel width. From the experimental data, the measured transverse volume fraction profiles were no longer wall-peaked after $x/L > 0.5$. This implies the presence of large bubbles, which are unaccounted for in the NPHASE-CMFD simulations. As such, results are only presented for the first half of the channel.



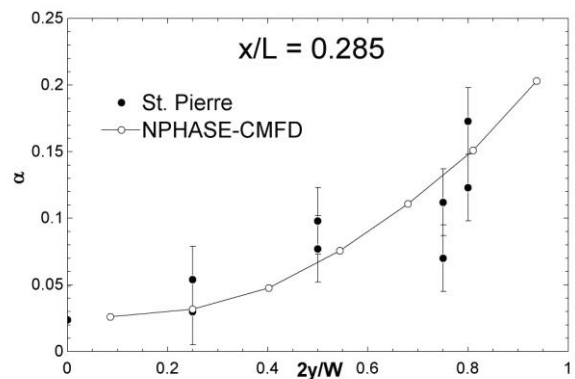
(a) average vapor volume fraction



(b) transverse vapor volume fraction at $x/L = 0.164$



(c) transverse vapor volume fraction at $x/L = 0.225$



(d) transverse vapor volume fraction at $x/L = 0.285$

Figure 4. Results for the experiment of St. Pierre (transverse profiles are presented along the $W = 11.1$ mm width of the channel where y is distance from the center)

The average vapor volume fraction shows excellent agreement between the NPHASE-CMFD predictions and the experimental data and the transverse profiles are quite reasonable as well. At $x/L = 0.164$, the vapor volume fraction profile predicted by the subcooled boiling model is significantly lower than the measured values near the center of the channel. This is shown in Figure 4b. This is consistent with what is shown in Figure 4a, where the predicted average volume fraction is less than the experimentally observed value. However, this data point does not align well with the trend of the neighboring data points and may be artificially high. It is likely that the experimental measurement of vapor volume fraction near the center of the channel does not reflect a true ensemble average.

All simulations have been performed at steady-state using the coupled solver in NPHASE-CMFD with the default numerical schemes. This includes a hybrid advection scheme for all equations. Convergence was typically governed by the RMS change in the volume fraction and an absolute residual of, at most, 10^{-6} was used. Although, due to the relatively small wall time required for the 2D simulations, it was not uncommon for residuals for all variables to reach machine-zero at convergence.

4. RESULTS OF PARAMETRIC SENSITIVITY TESTING

4.1. Bubble lift-off diameter

Because of the model's strong dependence on an accurate estimate of the bubble lift-off size and the inability to provide a reasonable a priori estimate, parametric testing was performed to demonstrate its

effect on the overall model predictions. Simulations were performed for the four experiments for a range of bubble lift-off diameters to determine a reasonable estimate. The extreme results (i.e. the max and min bubble lift-off diameters that were tested) are shown for Bartolomei's experiment and for Rouhani's experiment in Figure 5.

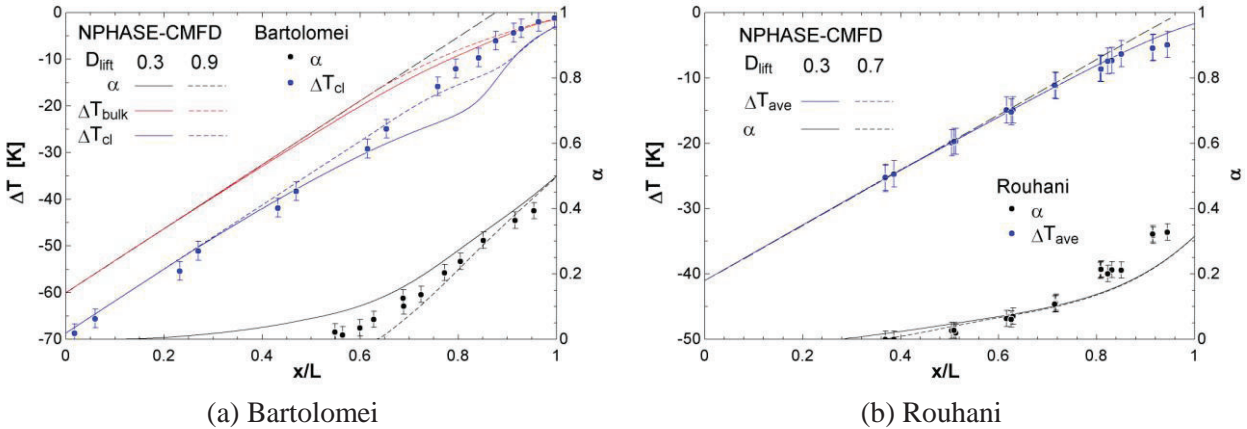


Figure 5. Sensitivity to bubble lift-off diameter

For the experiment of Bartolomei, it can be seen that the range of lift-off diameter tested had a significant effect on the point of net vapor generation. This is expected since the bubble lift-off diameter directly controls how far into the flow a standing bubble protrudes and, consequently, the liquid subcooling that the bubble is exposed to. The larger lift-off diameter protrudes farther away from the wall, where the liquid is much cooler allowing for complete condensation farther down the channel. The bubble lift-off diameter also had an effect on the centerline temperature. It was previously mentioned that the lower temperature predicted by NPHASE-CMFD is caused by an insulating effect. This is caused by vapor entrainment, which reduces the local shear and thus the turbulent generation. The smaller bubbles lead to a higher vapor volume fraction, which causes more entrainment of the liquid and reduces the generation of turbulent kinetic energy practically to zero, effectively insulating the center of the channel from the heating at the wall.

Interestingly, the experiment of Rouhani was insensitive to the bubble lift-off diameter. It does have some effect on the point of net vapor generation, but it is minor. This is likely due to the flow conditions being significantly different compared to Bartolomei's experiment. The mass flux is higher, the inlet subcooling is less, and the heat flux is much less. These factors lead to a higher condensation heat transfer coefficient, combined with a much flatter radial temperature profile for the liquid.

4.2. Grid sensitivity

Results of a grid independence study are shown in Figure 6 for Bartolomei's experiment. The grids used vary both in radial and axial spacing. The coarse grid consists of 7 nodes across the radius of the channel, 1000 nodes along the axis, and uses a next-to-wall node thickness equal to a bubble diameter, corresponding to a y_p^+ value of about 135. The fine grid consists of 10 nodes across the radius, 1600 nodes along the axis and uses a much thinner next-to-wall node spacing corresponding to a y_p^+ value of 50. Both values of y_p^+ are consistent with HRN turbulence model. It can be seen that practically no difference is observed in the presented result, with the exception of the near-wall node liquid subcooling. This is expected to be different, since the node represents a different location in the radial temperature profile. Similar testing was performed for all four experiments and grid independence was achieved.

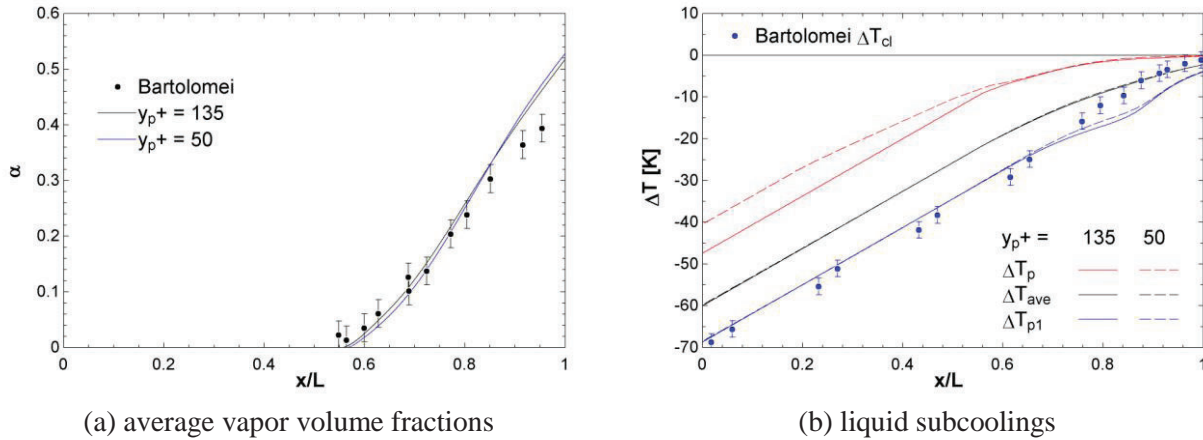


Figure 6. Grid sensitivity comparison

5. CONCLUSIONS

A novel approach for simulation of forced convection boiling has been proposed which accounts for both vapor generation and condensation on a heated wall. It has been implemented in NPHASE-CMFD with phenomenological models for interfacial heat, mass, and momentum transfer to produce a complete model of subcooled boiling.

Comparisons of model predictions to experimental data show quite good agreement. The ability of the model to well-predict radial and transverse distributions of both vapor volume fraction as well as liquid subcooling is quite significant. This indicates that the heat and mass transfer models as well as the interfacial force models are well formulated.

The overall model is still shown to be somewhat sensitive to the bubble diameter at lift-off. However, it was demonstrated that appropriate values for this can be estimated *a priori*. In addition, parametric testing demonstrates that at high flow rates, this sensitivity is significantly diminished.

REFERENCES

1. D. R. Shaver, S. P. Antal, and M. Z. Podowski, "Modeling and analysis of interfacial heat transfer phenomena in subcooled boiling along PWR coolant channels," in Proc. 15th Int. Topical Meeting on Nuclear Reactor Thermal-Hydraulics (NURETH), Pisa, Italy, May 2013, paper no. 586.
2. G. G. Bartolomei and V. M. Chanturiya, "Experimental study of true void fraction when boiling subcooled water in vertical tubes," Thermal Eng., vol. 14, no. 2, pp. 123–128, Aug. 1967.
3. S. Z. Rouhani, "Void measurements in the regions of sub-cooled and low-quality boiling," Aktiebolaget Atomenergi, Stockholm, Sweden, Tech. Rep. AE-239, 1966.
4. C. C. St. Pierre, "Frequency-response analysis of steam voids to sinusoidal power modulation in a thin-walled boiling water coolant channel," Argonne National Laboratory, Chicago, IL, Tech. Rep. ANL-7041, 1965.
5. W. Yao and C. Morel, "Volumetric interfacial area prediction in upward bubbly two-phase flow," Int. J. Heat Mass Transfer, vol. 47, no. 2, pp. 307–328, Jan. 2004.
6. N. Kurul and M. Z. Podowski, "On the modeling of multidimensional effects in boiling channels," in Proc. 27th Nat. Heat Transfer Conf., Minneapolis, MN, 1991, pp. 30–40.
7. T. H. Lee, G. C. Park, and D. J. Lee, "Local flow characteristics of subcooled boiling flow of water in a vertical concentric annulus," Int. J. Multiphase Flow, vol. 28, no. 8, pp. 1351–1368, Aug. 2002.

8. E. Krepper, B. Koncar, and Y. Egorov, "CFD modelling of subcooled boiling – concept, validation and application to fuel assembly design," *Nucl. Eng. and Design*, vol. 237, no. 7, pp. 716–731, Apr. 2007.
9. E. Chen, Y. Li, and X. Cheng, "CFD simulation of upward subcooled boiling flow of refrigerant-113 using the two-fluid model," *Applied Thermal Eng.*, vol. 29, no. 11, pp. 2508–2517, Aug. 2009.
10. M. Ishii and T. Hibiki, *Thermo-Fluid Dynamics of Two-phase Flow*, 2nd ed. New York, NY: Springer, 2006.
11. S. P. Antal, *NPHASE-CMFD User Manual*, Interphase Dynamics LLC, Schenectady, NY, 2002.
12. S. P. Antal, S. M. Ettore, R. F. Kunz, and M. Z. Podowski, "Development of a next generation computer code for the prediction of multicomponent multiphase flows," in *Proc. Int. Meeting Trends Numerical and Physical Modeling for Industrial Multiphase Flow*, Cargese, France, 2000, pp. 27–29.
13. E. A. Tselischeva, S. P. Antal, M. Z. Podowski, G. D., M. Beyer, and D. Lucas, "Analysis of developing gas/liquid two-phase flows," in *Proc. 7th Int. Conf. Multiphase Flow (ICMF)*, Tampa, FL, May 2010, paper no. 16.4.2.
14. F. Behafarid, D. R. Shaver, I. A. Bolotnov, K. Jansen, S. P. Antal, and M. Z. Podowski, "Coupled DNS/RANS simulation of fission gas discharge during loss-of-flow accident in GEN-IV sodium fast reactor," *J. Nucl. Technology*, vol. 181, no. 1, pp. 44 – 55, Jan. 2013.
15. Y. Sato and K. Sekoguchi, "Liquid velocity distribution in two-phase bubble flow," *Int. J. Multiphase Flow*, vol. 2, no. 1, pp. 79–95, June 1975.
16. S. P. Antal, R. T. Lahey, and J. E. Flaherty, "Analysis of phase distribution in fully developed laminar bubbly two-phase flow," *Int. J. Multiphase Flow*, vol. 17, no. 5, pp. 635–652, Sept. 1991.
17. M. Ishii and N. Zuber, "Drag coefficient and relative velocity in bubbly, droplet, or particulate flows," *Amer. Inst. Chem. Eng. J.*, vol. 25, no. 5, pp. 843–855, Sept. 1979.
18. I. Zun, "The Transverse Migration of Bubbles Influenced by Walls in Vertical Bubbly Flow," *Int. J. Multiphase Flow*, vol. 6, pp. 583-588, 1980.
19. D. R. Shaver, "Development of a Mechanistic Model for Forced Convection Subcooled Boiling," Ph.D. dissertation, Dept. of Mech., Aerospace, and Nucl. Eng., Rensselaer Polytechnic Inst., Troy, NY, 2014.
20. H. Jiao and M. Z. Podowski, "An analysis of multidimensional models of gas/liquid flows," in *Transactions Vol. 107 American Nuclear Society Winter Meeting*, San Diego, CA, Nov. 2012, pp. 1393–1394.
21. S. K. Wang, S. J. Lee, O. C. Jones, and R. T. Lahey, "3-d turbulence structure and phase distribution measurements in bubbly two-phase flows," *Int. J. Multiphase Flow*, vol. 13, no. 3, pp. 327–343, May 1987.
22. T. L. Gallaway, "Modeling of flow and heat transfer for fluids at supercritical conditions," Ph.D. dissertation, Dept. of Mech., Aerospace, and Nucl. Eng., Rensselaer Polytechnic Inst., Troy, NY, 2011.
23. Y. M. Chen and F. Mayinger, "Measurement of heat transfer at the phase interface of condensing bubbles," *Int. J. Multiphase Flow*, vol. 18, no. 6, pp. 877 – 890, Nov. 1992.
24. W.-C. B. V. Cuemern-Lindenstjerna, "Bubble departure diameter and release frequencies during nucleate pool boiling of water and aqueous NaCl solution," in *Heat Transfer in Boiling*, E. Hahne and U. Grigull, Eds. Salem, MA: Academic Press, 1977.
25. M. K. Jensen and G. J. Memmel, "Evaluation of bubble departure diameter correlations," in *Proc. 8th Int. Heat Transfer Conf.*, vol. 4, 1986, pp. 1907–1912.
26. H. C. Unal, "Maximum bubble diameter, maximum bubble growth time and bubble growth rate during subcooled nucleate flow boiling of water up to 17.7 mm/m²," *Int. J. Heat Mass Transfer*, vol. 19, no. 6, pp. 643 – 649, June 1976.
27. R. Sugrue and J. Buongiorno, "A modified force-balance model for predicting bubble departure diameter in subcooled flow boiling," in *Proc. 15th Int. Topical Meeting on Nuclear Reactor Thermal-Hydraulics (NURETH)*, Pisa, Italy, May 2013, paper no. 124.